

A Superior High Energy Density Biocidal Agent Achieved with a 3D Metal-Organic Framework

jichuan Zhang, Zhenye Zhu, Mingqing Zhou, Jiaheng Zhang, Joseph P. Hooper, and Jean'ne M. Shreeve

ACS Appl. Mater. Interfaces, **Just Accepted Manuscript** • DOI: 10.1021/acsami.0c12251 • Publication Date (Web): 13 Aug 2020

Downloaded from pubs.acs.org on August 13, 2020

Just Accepted

“Just Accepted” manuscripts have been peer-reviewed and accepted for publication. They are posted online prior to technical editing, formatting for publication and author proofing. The American Chemical Society provides “Just Accepted” as a service to the research community to expedite the dissemination of scientific material as soon as possible after acceptance. “Just Accepted” manuscripts appear in full in PDF format accompanied by an HTML abstract. “Just Accepted” manuscripts have been fully peer reviewed, but should not be considered the official version of record. They are citable by the Digital Object Identifier (DOI®). “Just Accepted” is an optional service offered to authors. Therefore, the “Just Accepted” Web site may not include all articles that will be published in the journal. After a manuscript is technically edited and formatted, it will be removed from the “Just Accepted” Web site and published as an ASAP article. Note that technical editing may introduce minor changes to the manuscript text and/or graphics which could affect content, and all legal disclaimers and ethical guidelines that apply to the journal pertain. ACS cannot be held responsible for errors or consequences arising from the use of information contained in these “Just Accepted” manuscripts.

A Superior High Energy Density Biocidal Agent Achieved with a 3D Metal-Organic Framework

Jichuan Zhang,^{1,2,3} Zhenye Zhu,² Mingqing Zhou,² Jiaheng Zhang,^{2,3*} Joseph P. Hooper,⁴ Jean'ne M. Shreeve^{1*}

¹Department of Chemistry, University of Idaho, Moscow, Idaho 83844-2343, USA.

²Research Centre of Flexible Printed Electronic Technology, Harbin Institute of Technology, Shenzhen, 518055, China.

³Zhuhai Institute of Advanced Technology Chinese Academy of Sciences, Biomaterials Research Center, Zhuhai, 519003, China.

⁴Department of Physics, Naval Postgraduate School, Monterey, California 93943, United States

Supporting Information

Keywords: 3D Metal-Organic Framework, biocidal agent, energetic materials, high energy density, iodine

ABSTRACT: A significant number of challenges are encountered when developing biocidal agents with high throwing capacity for biosafety applications. Now a three-dimensional metal-organic framework (3D MOF) {**MOF (2)**, [Cu(atrz)(IO₃)₂]_n (atrz = 4,4'-azo-1,2,4-triazole)} was obtained by using a post-synthetic method from **MOF (1)** {[Cu(atrz)₃(NO₃)₂]_n}. Benefitting from the oxygen-rich and small volume of the iodate (IO₃) ligands (2.73 Å) in **MOF (2)** compared to the atrz ligand (7.70 Å) in **MOF (1)**, the density of **MOF (2)** is 3.168 g cm⁻³, nearly twice that of its precursor. Its detonation velocity of 7271 ms⁻¹ exceeds that of TNT (trinitrotoluene) and its detonation pressure of 40.6 Gpa is superior to HMX (1,3,5,7-tetranitro-1,3,5,7-tetrazoctane, 39.2 Gpa), which are the highest detonation properties for a biocidal agent. Its superior detonation performance results in its main product, I₂, being distributed over a wide area markedly reducing the diffusion of harmful microorganisms. This study offers novel insight not only for high energy density materials but also for huge potential applications as biocidal agents.

INTRODUCTION

Development in modern science and technology has allowed people to live in environments with increased biosafety relative to the previous century. Frequent occurrences of bio-crises cause widespread disasters for people, animals and the environment.^{1, 2} These crises result from various reasons including the use of bioweapons by extremists, leakage of bioagents from storage, and outbreaks of organisms and toxins (such as SARS, Ebola, H7N9, and African Swine fever).³⁻⁸ For example, in 2001, a series of letters containing anthrax spores were sent by mail in the US. In the process, 22 people were seriously injured, five of whom died, and probably thousands were contaminated and advised to use antibiotics for an extended period of time.⁹ At the beginning of 2020, the outbreak of COVID-19 has caused many deaths all over the world.¹⁰ The growth in the numbers of bio-crises have led to an increase in the scope and magnitude of highly infectious diseases.^{11,12} Traditional biocidal methods require a significant effort to distribute anti-biological agents. However, this tends to be inefficient, susceptible to infection for people, and these materials cannot be distributed over a large range, especially in those places that are reached with difficulty. Preventing diffusion of these harmful microorganisms and improving their rapid elimination on a large scale is an enormous challenge.

Iodine is an efficient biocidal agent for bacteria, fungi, yeasts, viruses, spores, and protozoan parasites (a 99.999% kill in 10 min at 25 °C).¹³ However, since it sublimates readily, elemental iodine itself is not useful as an anti-biological agent. Until recently, the emergence of iodine-containing energetic compounds, which can kill harmful microorganisms by releasing I₂ upon initiation, was a milestone for both energetic materials as well as anti-biological agents.¹⁴⁻²⁷ These compounds not only improved the biocidal efficiency, but also precluded the sublimation of iodine in the anti-biological agents. Nevertheless, the drawbacks of the current iodine-

containing energetic agents are notable including 1) the detonation performances of all the reported iodine-containing compounds are low {only one compound, 3,3,3-trinitropropyl-1-ammonium periodate is higher than that of TNT (2,4,6-trinitrotoluene), while its iodine content is only 32.9%, and its decomposition temperature is only 138 °C,²⁷ which is unsuitable for a biocidal agent; 2) The energy level of most iodine-containing compounds is too low to allow ignition, and the mixture of iodine-containing agents with explosives complicates the process of energetic iodine-containing agents and may likely result in accidents; and 3) Nearly all the iodine-containing agents are obtained through organic syntheses that result from costly multi-step reactions and that produce organic waste which is not environmentally friendly. Therefore, developing novel iodine-containing agents that exhibit superior detonation properties by a simple method is worthwhile as well as being significantly challenging.

Three-dimensional metal-organic frameworks (3D MOFs) have been utilized extensively in catalysts, drug transportation, absorption and separation since the beginning of the 21st century due to their excellent porosity.^{28,29} Energetic 3D MOFs are a unique type of 3D MOFs which are comprised of energetic nitrogen-rich ligands and metal ions.³⁰⁻³² Energetic 3D MOFs have drawn significant attention since the first report of **MOF (1)**, [Cu(atrz)₃(NO₃)₂]_n (atrz = 4,4'-azo-1,2,4-triazole) because of its high thermal stability and low sensitivity.³³ Just as with traditional energetic materials, the primary aim of energetic 3D MOFs is to achieve high energy density (minimum porosity). However, their detonation properties and densities still have not been realized because 1) the presence of two or three ligands in unit cell leads to a low oxygen balance in the energetic 3D MOFs, even with oxygen-rich anions (NO₃, ClO₄), and 2) the empty volumes of most energetic 3D MOFs are higher than those organic compounds leading to an energetic density even lower than that of the organic compounds. For example, the oxygen balance of **MOF (1)** is -58.82%, and the

length of atrz is 7.70 Å, making the density of **MOF (1)** only 1.64 g cm⁻³, which is even lower than most organic energetic compounds (Figure S1). Although several strategies have been employed including introducing more energetic molecules or anions in the holes of 3D MOFs or replacing ligands with smaller volume nitrogen-rich ligands in order to increase the energetic densities of 3D MOFs, the desired results are still not obtained.³⁴⁻³⁷ Hence, employing a novel strategy to change this situation is necessary.

Recently, a post-synthetic method has become increasingly interesting for preparing MOFs because the conditions employed are mild which facilitates the investigation of their synthesis mechanisms.³⁸ In addition, the IO₃⁻ anion serves both roles of being iodine- and oxygen rich. Due to the larger atomic radius and lower electronegativity of iodine relative to fluorine and chlorine anions, the coordination ability of the IO₃⁻ anion is strong.^{39,40} Thus, if the IO₃⁻ anion replaces one or two nitrogen-rich ligands in an energetic 3D MOF, the oxygen balance, density and energy level of the new MOF will be increased greatly, and the new MOF will exhibit a biocidal effect upon decomposition. Now KIO₃ was chosen to exchange with **MOF (1)**,

and the properties including crystal structure, energetic performance and biocidal effect of the resulting MOF were studied extensively.

RESULTS AND DISCUSSION

Synthesis and single-crystal structure. **MOF (1)** was immersed in a solution of KIO₃ (2.1 M) for 24 hours at room temperature. The color of the crystals changed from blue to baby blue (S2, Supporting information). The resulting crystal structure was determined by X-ray diffraction to be monoclinic (P21/c), with one Cu, one atrz ligand, and two IO₃⁻ anions in each unit cell, **MOF (2)** [Cu(atrz)(IO₃)₂]_n. Two atrz ligands which play a counter ion role in **MOF (1)** were replaced by IO₃⁻ anions in the same role. The coordination of Cu in **MOF (2)** approaches a regular octahedron and is similar to that found in **MOF (1)**. Due to the diameter of IO₃⁻ (2.73 Å) which is less than that of atrz, the length of the two diagonals of the rectangle in **MOF (2)** was found to be only 20.13 Å which is still shorter than a single diagonal in **MOF (1)** (Figure 1). In addition, the lengths of Cu-N and Cu-O bonds of 2 are 1.997 Å, 1.994 Å, and 2.318 Å, respectively, which are shorter

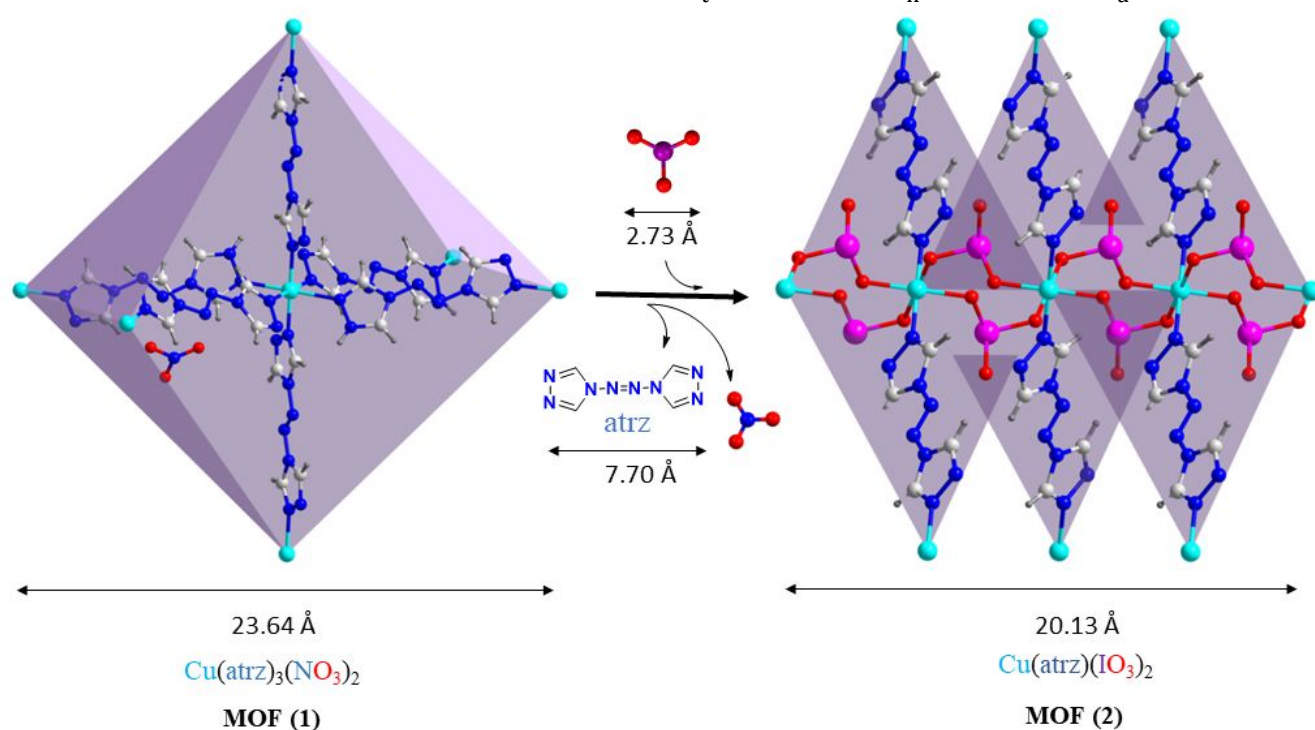


Figure 1. The change of crystal size between **MOF (1)** and **MOF (2)**

the three Cu-N bonds (2.009, 2.030, and 2.381 Å, respectively) in **MOF (1)**, correspondingly. The shorter Cu-N/O coordination bonds and IO₃ ligands in **MOF (2)** relative to **MOF (1)** give rise to a void volume (inverse with packing index) of **MOF (2)** as low as 22.3% (packing index 77.7%, Figure S1a). The closer packing of **MOF (2)** compared to **MOF (1)** is seen from Figure 2A and 2D. Meanwhile, the characterizations of SEM and EDX (Figure 2B-2C, 2E-2F and S3) show distinct differences between **MOF (1)** and **MOF (2)**. The **MOF (2)** is the second lowest void volume based on 485 3D MOFs of transition metals, and it is just slightly higher than that of the lowest one (22.0%, [CuBT(H₂O)]_n, BT = 5,5'-bistetrazolate).⁴¹ The packing index of **MOF (2)** is not only higher than **MOF (1)** (68.7%), but also higher than the majority of the energetic organic compounds (Figure S1b). The density of **MOF (2)** is 3.168 g cm⁻³, which is

almost twice the value of its precursor (1.68 g cm⁻³, 173 K). In order to study the process and mechanism of exchange, **MOF (1)** was added to solutions which contained 0.2/0.5/1.0/1.5/2.0/3.0 M of KIO₃ at room temperature, respectively (S2). The resulting samples changed gradually from blue to baby blue over 24 hours. After filtering and drying, these samples were characterized by FT-IR (Fourier transform infrared spectroscopy) (Figure 3A), XRD (X-ray diffraction) (Figure 3B). In FT-IR spectra, the characteristic peak of the NO₃⁻ anion is at ~ 1385 cm⁻¹, and that of the IO₃⁻ anion is at ~ 750 cm⁻¹. With a gradual increase in the proportion of KIO₃, the NO₃⁻ anions of **MOF (1)** were gradually replaced by IO₃⁻. This led to a decrease in the intensity of NO₃⁻ in these samples, and an enhanced intensity of IO₃⁻. Similarly, when the molar ratios between KIO₃ and **MOF (1)** increased gradually, the XRD

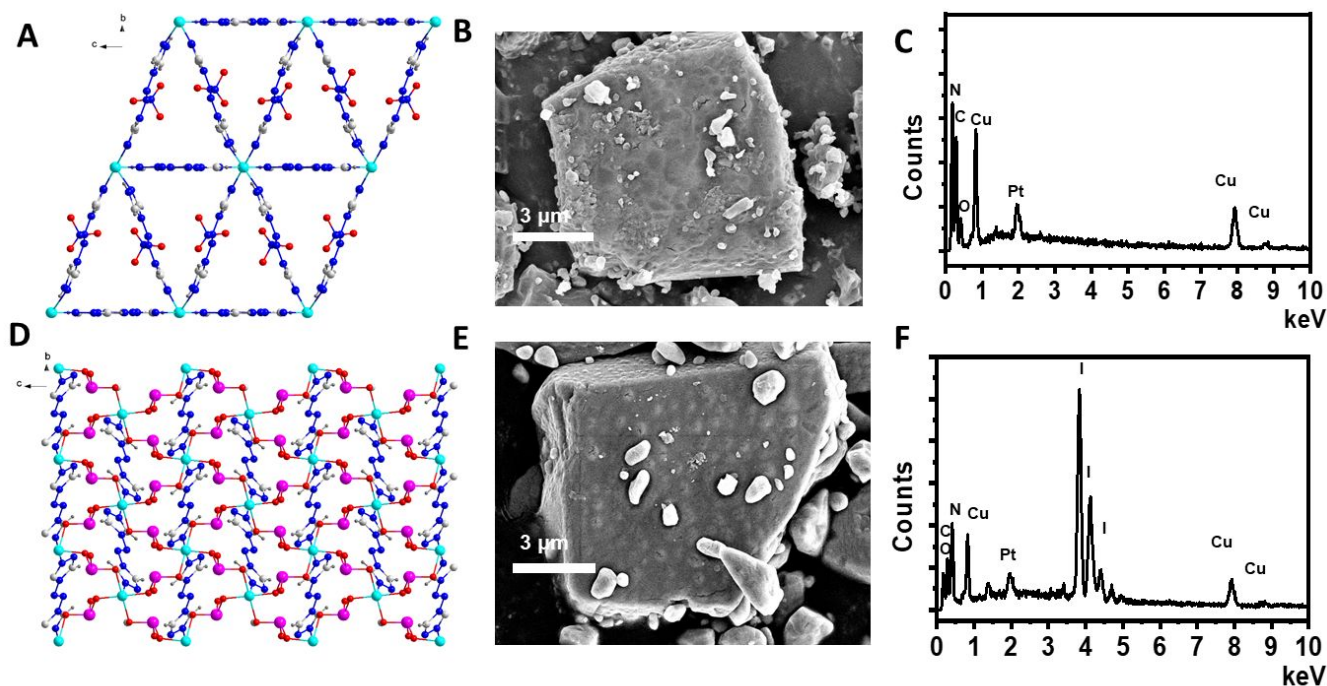


Figure 2. A,D) The packing structure of **MOF (1)** and **MOF (2)** view from a axes, respectively; B,E) SEM (scanning electron microscope) of **MOF (1)** (1) and **MOF (2)**, respectively; C, F) EDX (energy dispersive X-ray spectroscopy) scans of **MOF (1)** and **MOF (2)**, respectively.

characteristic peaks (2θ : 8.6, 11.1, 11.7, 15.1, 17.3, 22.0, 22.6, 23.6, 26.2, 30.1, 33.9) of **MOF (1)** got increasingly weaker, while the characteristic peaks of **MOF (2)** (2θ : 9.5, 16.1, 18.8, 21.3, 23.0, 24.4, 25.0, 27.8, 32.4, 37.8, 39.0) were found to get stronger. Finally, the combination of elemental analysis, FT-IR and XRD tests, shows that when the molar ratio between KIO_3 and **MOF (1)** is 2:1, crystalline **MOF (1)** was nearly converted completely into **MOF (2)**. When this ratio was increased to 3:1, **MOF (1)** was 100% changed into **MOF (2)**, which is supported by elemental analysis. Calculations based on NBO charge distribution and coordination bond energy (S4-S5) were conducted to investigate the driving force of the exchange. The calculated results show that the charge density of the O atom (IO_3^-) was -1.227, which is

considerably higher than that of NO_3^- (-0.561), suggesting that the possibility of the formation of a coordination bond between IO_3^- and Cu is markedly higher than between Cu and NO_3^- . The calculated energies of the three Cu-N bonds in **MOF (1)** are 406.2, 409.5 and 254.0 kJ mol^{-1} , respectively, which are much lower than the two Cu-O bonds (673.1 and 654.1 kJ mol^{-1}) and the one Cu-N (614.9 kJ mol^{-1}) of **MOF (2)**. These results show that exchange between **MOF (1)** and KIO_3 occurs readily, and that IO_3^- enhances the stability of **MOF (2)** relative to that of **MOF (1)**. The structure of **MOF (2)** is strengthened greatly, which is also supported by HPLC (High Performance Liquid Chromatography) tests. The HPLC tests of solubility show that **MOF (1)** is ~ 17 times (7.06 g l^{-1}) more soluble in water than **MOF (2)** (S6). The solubility of **MOF (2)**

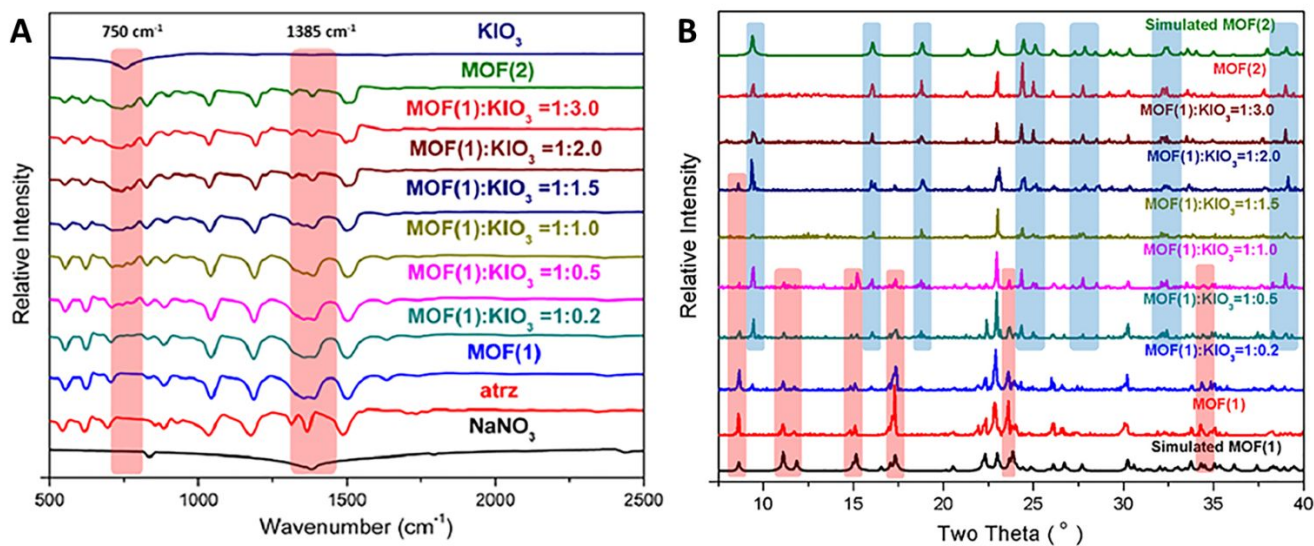


Figure 3. Transformations of FT-IR (A) and XRD (B) during post-synthesis.

was calculated to be 0.42 g l^{-1} , showing that it is slightly soluble in water. Given the above results of calculations and HPLC tests, **MOF (2)** could be synthesized from hot water ($80\text{ }^\circ\text{C}$) in 30 seconds on a large scale using atrz, $\text{Cu}(\text{NO}_3)_2$ and KIO_3 in a molar ratio 1:1:2 (S7).

Physicochemical properties. Excellent thermal stability and acceptable sensitivity values are basic requirements for promising energetic materials as well as biocidal agents. The decomposition temperature (onset) of **MOF (2)** is $267\text{ }^\circ\text{C}$ measured at a nitrogen flow rate of $5\text{ }^\circ\text{C min}^{-1}$ using a Differential Scanning Calorimeter (DSC Q2000, S8). This value is not only higher than those of all the IO_3^- -containing organic compounds (their thermal stabilities are $\leq 190\text{ }^\circ\text{C}$),²⁴ but also higher than that of the classic explosive RDX (cyclotrimethylenetrinitramine, $T_d = 210\text{ }^\circ\text{C}$), and it is comparable with HMX (cyclotetramethylenetetranitramine, $T_d = 280\text{ }^\circ\text{C}$). Sensitivities to impact and friction were determined based on the BAM Standard,^{42, 43} which gave impact and friction sensitivities of **MOF (2)** at 18 J and 60 N (S9), respectively. These are considerably less sensitive than most reported IO_3^- examples. Higher thermal stability and lower sensitivity than those of IO_3^- -based organic compounds should arise from the strong coordination bonds in **MOF (2)**. It should be noted that IO_3^- increases the oxygen balance of **MOF (2)** to -12.47% from -57.65% for **MOF (1)**. This is also higher than that of TNT (-74.00%), RDX (-21.62%) and HMX (-21.62%). The increased oxygen balance is very helpful in improving the detonation performance.

The heat of combustion of **MOF (2)** was determined to be 3469 kJ mol^{-1} with an Oxygen Bomb Calorimeter (PARR 1341EB, BOMB CALORI PLAIN). Its heat of formation was calculated to be 1181 kJ mol^{-1} using Hess's law (S9), which arises from the high heat of formation of the nitrogen-rich ligand⁴⁴ and the strong coordination bonds. With an experimental density of 3.11 g cm^{-3} at room temperature and heat of formation in hand, the detonation velocity of **MOF (2)** were calculated by Cheetah 8.0 to be 7271 ms^{-1} , which is the highest detonation velocity among all reported iodine-

containing compounds and superior to that of TNT (6881 m^{-1}), and its detonation pressure is 40.61 GPa exceeding that of HMX (39.50 GPa). This is higher than all reported detonation pressure values of iodine-containing compounds.¹⁴⁻²⁷ The surprisingly elevated detonation properties of **MOF (2)** are the result of an ideal combination of a high heat of formation, high density and excellent oxygen balance, which could disperse the explosion products over a larger area.

The iodine content of **MOF (2)** is 43.98% . When it was initiated, 43.17% I_2 would be released by **MOF (2)**, which was predicted by Cheetah 8.0 (S10 and Cheetah calculation file). This was observed as a purple cloud with a high-speed camera with an interval of 0.2 ms (Figure 4A-4D). The iodine released plays the main role in the bactericidal effect, which was proved by biocidal tests in both solid and liquid phases. The small amount of Cu as well as CuO formed quickly after explosion could also be helpful as biocides.^{45,46} The solid biocide tests were conducted according to previous work.¹⁵ *Escherichia coli* (Ec), *Staphylococcus aureus* (Sa) and *Pseudomonas aeruginosa* (Pa) were chosen as representatives of harmful microorganisms because they are widely distributed on the earth and easily infect people.⁴⁷⁻⁴⁹ The explosion products of **MOF (2)** were collected in an oxygen bomb with water and added to five circular papers (diameter = 3 mm) with varying amounts of decomposed samples of **MOF (2)** ($10\text{ }\mu\text{g}$, $20\text{ }\mu\text{g}$, $30\text{ }\mu\text{g}$, $40\text{ }\mu\text{g}$, $50\text{ }\mu\text{g}$ portions, respectively). The circles were placed in the culture medium. The results showed that when the **MOF (2)** concentration was $30\text{ }\mu\text{g}$, all bacteria were annihilated in 30 minutes (Figure 4E, and S11). Based on the size of circles (28.26 mm^2), the effective biocidal quality of **MOF (2)** for 1 km^2 would be 1.06 ton . Given that the harmful microorganisms can also exist in water, the biocidal tests of these three bacteria were conducted in aqueous solutions. Products of **MOF (2)** were added into three vials, respectively, which contain these three breeding bacteria. Half an hour later, bacteria in each of the three vials were killed completely (Figure 4F-4G), and the minimum biocidal concentrations responding to **MOF (2)** for these three bactericides are the same, at 3 mg mL^{-1} . Although

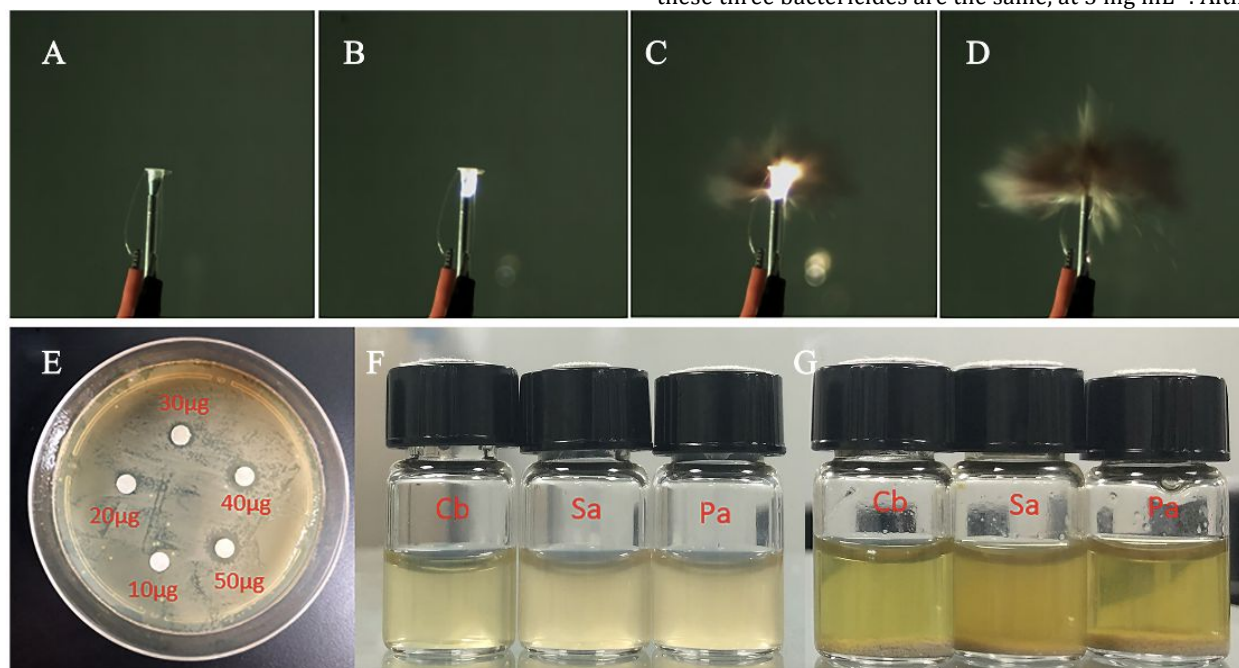


Figure 4. (A-D) Images of the explosion initiation captured by high-speed camera with an interval of 0.2 ms ; (E) the bactericide effect on *Escherichia coli*; (F) suspension solutions of three breeding bacteria; (G) the addition of the explosion products of **MOF (2)** into three breeding bacteria solutions in 30 minutes (dead bacteria: precipitate on the bottom of the culturing bottles).

the biocidal capacity of **MOF (2)** is slightly lower than that of DIDNPT (2,6-diiodo-3,5-dinitro-4,9-dihydrodipyrzolo [1,5-a:5',1'-d][1,3,5]triazine, (Table S5)),¹⁵ which could kill bacteria over 1 km² with about 0.8 ton, the detonation performance of **MOF (2)** is considerably higher than that of DIDNPT and could distribute the products of **MOF (2)** to a larger area to kill much more harmful bacteria.

CONCLUSION

In summary, iodine-containing 3D **MOF (2)** was obtained by methods of exchange and synthesis, and the exchange process and mechanism were studied extensively. Distinct from the reported 3D MOFs, the short and strong coordination ability of IO₃⁻ anions play both the role of ligand as well as counter ion. This results in 1) the oxygen balance of **MOF (2)** at -12.47%, which is higher than those of classic explosives such as TNT, RDX and HMX and its precursor **MOF (1)**; 2) the density of **MOF (2)** is 3.168g cm⁻³, which is nearly twice relative to **MOF (1)**; and 3) high thermal stability and low sensitivity among iodate compounds. High density, high heat of formation, and a less negative oxygen balance give rise to a detonation velocity for **MOF (2)** of 7271m s⁻¹, which is the highest detonation velocity found for iodine-containing compounds. Additionally, its detonation pressure is higher than that of HMX. Superior detonation performance combined with excellent biocidal effects suggests that the explosion products including iodine (a biocide) could be distributed over a large area which will prevent the diffusion of harmful microorganisms through annihilation. This study provides a novel inroad into high energy density materials and potentially valuable biocidal agents in infection control.

EXPERIMENTAL SECTION

Safety Precautions. Although none of the energetic MOFs described herein have exploded or detonated in the course of this research, these materials should be handled with extreme care using the best safety practices.

General Methods. **MOF (1)** was prepared according to the literature.³² All other materials were commercially available and used without further purification. Powder X-ray diffraction (PXRD) patterns of the samples were analyzed with monochromatized Cu-K α ($\lambda = 1.54178 \text{ \AA}$) incident radiation by Bruker D8 Advance X-ray diffractometer operating at 40 kV voltage and 50 mA current. PXRD patterns were recorded from 5° to 80° (2 θ) at 298 K. IR spectra were recorded using KBr pellets with a FT-IR spectrometer (Thermo Nicolet AVATAR 370). Density was determined at room temperature by employing a Micromeritics AccuPyc II 1340 gas pycnometer. Decomposition (onset) temperatures were recorded using a dry nitrogen gas purge and a heating rate of 5 oC min⁻¹ on a differential scanning calorimeter (DSC, TA Instruments Q2000). Elemental analyses (C, H, N) were performed with a Vario Micro cube Elementar Analyser. Impact and friction sensitivity measurements were made using a standard BAM Fall hammer and a BAM friction tester.

X-ray Crystallography. Single blue block-shaped crystals of **MOF (2)** were used as received. A suitable crystal 0.12×0.12×0.08 mm³ was selected and mounted on a nylon loop with paratone oil on a Bruker APEX-II CCD diffractometer. The crystal was kept at a steady T = 173(2) K during data collection. The structure was solved with the ShelXT (Sheldrick, G.M. (2015). Acta Cryst. A71, 3-8) structure solution program using the Intrinsic Phasing solution method and by using Olex2 (Dolomanov et al., 2009) as the graphical interface. The model was refined with version 2018/3 of ShelXL (Sheldrick, Acta

Cryst. A64 2008, 112-122) using Least Squares minimization.

□ ASSOCIATED CONTENT

Supporting Information

Supplementary Information (Experimental method, additional figures and tables) is available in the online version of the paper (<http://pubs.acs.org>).

□ AUTHOR INFORMATION

Corresponding Author

jshreeve@uidaho.edu
zhangjiaheng@hit.edu.cn

Notes

The authors declare no competing financial interest.

ACKNOWLEDGMENT

Financial support of the Office of Naval Research (N00014-16-1-2089), and the Defense Threat Reduction Agency (HDTRA 1-15-1-0028) is gratefully acknowledged. This work was supported by the National Natural Science Foundation of China (21905069), the Shenzhen Science and Technology Innovation Committee (JCYJ20180507183907224, KQTD20170809110344233), Economic, Trade and Information Commission of Shenzhen Municipality through the Graphene Manufacture Innovation Center (201901161514).

REFERENCES

- (1) Boddie, C.; Watson, M.; Ackerman, G.; Gronvall, G. K. Assessing the Bioweapons Threat, *Science*, **2015**, 349(6250), 792-793.
- (2) Berger, K. M. What Life Scientists Should Know about Security Threats, *Science*, **2016**, 354(6317), 1237-1239.
- (3) Seelos, C. Lessons from Iraq on Bioweapons, *Nature*, **1999**, 398, 187-188.
- (4) Stenseth, N. C.; Atshabar, B. B.; Begon, M.; Belmain, S. R.; Bertherat, E.; Carniel, E.; Gage, K. L.; Leirs, H.; Rahalison, L. Plague: Past, Present, and Future, *PLoS Medicine*, **2008**, 5, 1.
- (5) Fouchier, R. A. M.; Kuiken, T.; Schutten, M.; Amerongen, G. V.; Doornum, G. J. J.; Hoogen, B. G. V.; Peiris, M.; Lim, W.; Stöhr, K.; Osterhaus, A. D. M. E. Koch's Postulates Fulfilled for SARS Virus, *Nature*, **2003**, 423, 240.
- (6) Feldmann, H.; Geisbert, T. W. Ebola Haemorrhagic Fever, *The Lancet*, **2001**, 377, 849-862.
- (7) Costard, S.; Wieland, B.; Glanville, W. D.; Jori, F.; Rowlands, R.; Vosloo, W.; Roger, F.; Pfeiffer, D. U.; Dixon, L. K. African Swine Fever: How Can Global Spread be Prevented? *Phil. Trans. R. Soc. B*, **2009**, 364, 2683-2696.
- (8) Riedel, S. Biological Warfare and Bioterrorism: a Historical Review, *Bumc Proceedings*, **2004**, 17, 400-406.
- (9) Jansen, H. J.; Breeveld, F. J.; Stijnis, C.; Grobusch, M. P. Biological Warfare, Bioterrorism, and Biocrime, *Clin. Microbiol. Infect.*, **2014**, 20: 488-496.
- (10) Huang, C., Wang, Y., Li, X., Ren, L., Zhao, J., Hu, Y., Zhang, L., Fan, G., Xu, J., Gu, X., Cheng, Z., Yu, T., Xia, J., Wei, Y., Wu, W., Xie, X., Yin, W., Li, H., Liu, M., Xiao, Y., Gao, H., Guo, L., Xie, J., Wang, G., Jiang, R., Gao, Z., Jin, Q., Wang, J., Cao, B. Clinical Features of Patients Infected with 2019 Novel Coronavirus in Wuhan, China. *The Lancet*, **2020**, 395 (10223), 497-506.
- (11) <https://www.ncbi.nlm.nih.gov/books/NBK493217/>, 08-12-2020.
- (12) Narayanan, N.; Lacy, C. R.; Cruz, J. E.; Nahass, M.; Karp, J.; Barone, J. A.; Hermes-DeSantis, E. R. Disaster

- Preparedness: Biological Threats and Treatment Options, *Pharmacol. Ther.*, **2018**, 38(2):217-234.
- (13) Kaiho, T. Iodine Chemistry and Applications; John Wiley & Sons, Inc.: New York, **2015**.
- (14) Agrawal, J. P.; Hodgson, R. D. Organic Chemistry of Explosives, John Wiley & Sons Ltd, Copyright **2007**.
- (15) Zhao, G.; He, C.; Zhou, W.; Hooper, J. P.; Imler, G. H.; Parrish, D. A.; Shreeve, J. M. Control of Biohazards: a High Performance Energetic Polycyclized Iodine-containing Biocide, *Inorg. Chem.* **2018**, 57, 8673-8680.
- (16) Chand, D.; He, C.; Hooper, J. P.; Mitchell, L. A.; Parrish, D. A.; Shreeve, J. M. Mono-and Diiodo-1, 2, 3-triazoles and Their Mono Nitro Derivatives, *Dalton Trans.*, **2016**, 45, 9684-9688.
- (17) Chand, D.; Shreeve, J. M. Versatile Synthesis and Promise, *Chem. Commun.*, **2015**, 51, 3438-3441.
- (18) Chand, D.; He, C.; Mitchell, L. A.; Parrish, D. A.; Shreeve, J. M. Electrophilic Iodination: a Gateway to High Iodine Compounds and Energetic Materials, *Dalton Trans.*, **2016**, 45, 13827-13833.
- (19) Zhao, G.; He, C.; Kumar, D.; Hooper, J. P.; Imler, G. H.; Parrish, D. A.; Shreeve, J. M. 1, 3, 5-Triiodo-2, 4, 6-trinitrobenzene (TITNB) from Benzene: Balancing Performance and High Thermal Stability of Functional Energetic Materials, *Chem. Eng. J.* **2019**, 378, 122119.
- (20) Chinnam, A. K.; Shlomovich, A.; Shamis, O.; Petrutik, N.; Kumar, D.; Wang, K.; Komarala, E. P.; Tov, D. S.; Sućeska, M.; Yan, Q. L.; Gozin, M. Combustion of Energetic Iodine-rich Coordination Polymer-Engineering of New Biocidal Materials, *Chem. Eng. J.*, **2018**, 350, 1084-1091.
- (21) Zhao, G.; He, C.; Kumar, D.; Hooper, J. P.; Imler, G. H.; Parrish, D. A.; Shreeve, J. M. Functional Energetic Biocides by Coupling of Energetic and Biocidal Polyiodo Building Blocks, *Chem. Eng. J.*, **2019**, 368, 244-251.
- (22) Zhao, G.; Kumar, D.; He, C.; Hooper, J. P.; Imler, G. H.; Parrish, D. A.; Shreeve, J. M. New Generation Agent Defeat Weapons: Energetic N,N' - Ethylene - Bridged Polyiodoazoles, *Chem. Eur. J.* **2017**, 23, 16753-16757.
- (23) He, C.; Zhang, J.; Shreeve, J. M. Dense Iodine - Rich Compounds with Low Detonation Pressures as Biocidal Agents, *Chem. Eur. J.*, **2013**, 19, 7503-7509.
- (24) He, C.; Hooper, J. P.; Shreeve, J. M. Iodine-rich Imidazolium Iodate and Periodate Salts: En Route to Single-based Biocidal Agents, *Inorg. Chem.* **2016**, 55, 12844-12850.
- (25) He, C.; Zhao, G.; Hooper, J. P.; Shreeve, J. M. Energy and Biocides Storage Compounds: Synthesis and Characterization of Energetic Bridged Bis(triiodoazoles), *Inorg. Chem.* **2017**, 56, 13547-13552.
- (26) He, C.; Parrish, D. A.; Shreeve, J. M. Alkyl Ammonium Cation Stabilized Biocidal Polyiodides with Adaptable High Density and Low Ppressure, *Chem. Eur. J.* **2014**, 20, 6699-6706.
- (27) Unger, C. C.; Klapötke, T. M.; Krumm, B. Unusual Energetic Periodate, Sulfate and Amino-bistetrazolate Salts of the Trinitropropylammonium Cation, *Z. Anorg. Allg. Chem.* **2020**, 646, 2-4.
- (28) Cook, T. R.; Zheng, Y.; Stang, P. J. Metal-organic Frameworks and Self-assembled Supramolecular Coordination Complexes: Comparing and Contrasting the Design, Synthesis, and Functionality of Metal-organic Materials, *Chem. Rev.* **2013**, 113, 734-777.
- (29) Lu, G.; Li, S.; Guo, Z.; Farha, O. K.; Hauser, B. G.; Qi, X.; Wang, Y.; Wang, X.; Han, S.; Liu, X.; DuChene, J. S.; Zhang, H.; Zhang, Q.; Chen, X.; Ma, J.; Loo, S. C. J.; Wei, W. D.; Yang, Y.; Hupp, J. T.; Huo, F. Imparting Functionality to a Metal-organic Framework Material by Controlled Nanoparticle Encapsulation. *Nature Chem.*, **2012**, 4(4), 310-316.
- (30) Zhang, J.; Shreeve, J. M. 3D Nitrogen-rich Metal-organic Frameworks: Opportunities for Safer Energetics, *Dalton Trans.*, **2016**, 45, 2363-2368.
- (31) McDonald, K. A.; Seth, S.; Matzger, A. J. Coordination Polymers with High Energy Density: An Emerging Class of Explosives, *Cryst. Growth Des.* **2015**, 15, 5963-5972.
- (32) Chen, S.; Jin, Y.; Xia, H.; Wang, K.; Liu, Y.; Zhang, Q. Synthesis of Fused Tetrazolo[1,5-b]pyridazine-based Energetic Compounds, *Energetic Materials Frontiers*, 2020, doi.org/10.1016/j.enmf.2020.05.001.
- (33) Li, S.; Wang, Y.; Qi, C.; Zhao, X.; Zhang, J.; Zhang, S.; Pang, S. 3D Energetic Metal-Organic Frameworks: Synthesis and Properties of High Energy Materials, *Angew. Chem. Int. Ed.* **2013**, 52, 14031 - 14035.
- (34) Du, Y.; Su, H.; Fei, T.; Hu, B.; Zhang, J.; Li, S.; Pang, S.; Nie, F. Structure-Property Relationship in Energetic Cationic Metal-Organic Frameworks: New Insight for Design of Advanced Energetic Materials, *Cryst. Growth Des.* **2018**, 18, 5896-5903.
- (35) Zhang, J.; Du, Y.; Dong, K.; Su, H.; Zhang, S.; Li, S.; Pang, S. Taming Dinitramide Anions within an Energetic Metal-organic Framework: A New Strategy for Synthesis and Tunable Properties of High Energy Materials, *Chem. Mater.* **2016**, 28, 1472-1480.
- (36) Huang, Y. Q.; Zhao, X. Q.; Shi, W.; Liu, W. Y.; Chen, Z. L.; Cheng, P.; Liao, D. Z.; Yan, S. P. Anions-directed Metal-mediated Assemblies of Coordination Polymers Based on the Bis(4, 4'-bis-1, 2, 4-triazole) Ligand, *Cryst. Growth Des.* **2008**, 8, 3652-3660.
- (37) Ding, B.; Wang, Y. Y.; Liu, S. X.; Wu, X. X.; Zhu, Z. Z.; Huo, J. Z.; Liu, Y. Y. A Series of Multi-dimensional Metal-organic Frameworks with Trans-4, 4' -azo-1, 2, 4-triazole: Polymorphism, Guest Induced Single-crystal-to-single-crystal Transformation and Solvatochromism, *CrystEngComm*, **2015**, 17, 5396-5409.
- (38) Cohen, S. M. Postsynthetic Methods for the Functionalization of Metal-organic Frameworks, *Chem. Rev.* **2012**, 112, 970-1000.
- (39) Li, G.; Shi, Z.; Liu, X.; Dai, Z.; Gao, L.; Feng, S. A New Inorganic-Organic Hybrid Copper Iodate with Potentially Large Void Volume, *Inorg. Chem.* **2004**, 43, 8224-8226.
- (40) Sun, C. F.; Hu, C. L.; Xu, X.; Yang, B. P.; Mao, J. G. Explorations of New Second-order Nonlinear Optical Materials in the Potassium Vanadyl Iodate System, *J. Am. Chem. Soc.* **2011**, 133, 5561-5572.
- (41) Chen, S.; Zhang, B.; Yang, L.; Wang, L.; Zhang, T. Synthesis, Structure and Characterization of Neutral Coordination Polymers of 5, 5'-bistetrazole with Copper (II), Zinc (II) and Cadmium (II): A New Route to Reconcile Oxygen Balance and Nitrogen Content of High-energy MOFs, *Dalton Trans.*, **2016**, 45, 16779-16783.
- (42) Standardization Agreement 4489 (STANAG 4489), Explosives, Impact Sensitivity Tests; NATO: Brussels, Belgium, **1999**.
- (43) Standardization Agreement 4487 (STANAG 4487), Explosives, Friction Sensitivity Tests; NATO: Brussels, Belgium, **2002**.
- (44) Xu, Y.; Wang, Q.; Shen, C.; Lin, Q.; Wang, P.; Lu, M. A Series of Energetic Metal Pentazolate Hydrates, *Nature*, **2017**, 549, 78-81.
- (45) Khan, S. T., Ahamed, M., Al-Khedhairi, A., Musarrat, J. Biocidal Effect of Copper and Zinc Oxide Nanoparticles on

Human Oral Microbiome and Biofilm Formation. *Mater. Lett.*, **2013**, 97, 67-70.

(46) Ruparelia, J. P., Chatterjee, A. K., Duttagupta, S. P., & Mukherji, S. Strain Specificity in Antimicrobial Activity of Silver and Copper Nanoparticles. *Acta Biomater.*, **2008**, 4(3), 707-716.

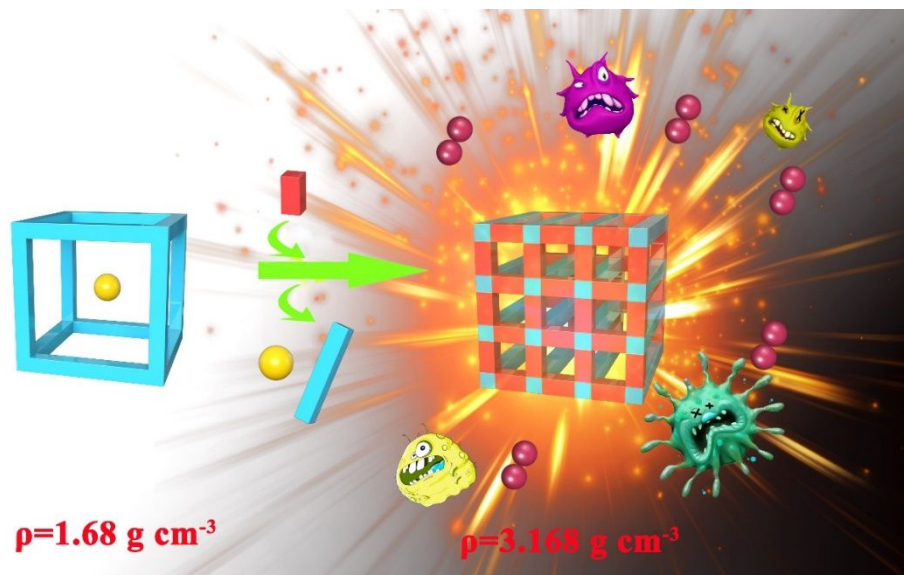
(47) Moran, G. J.; Krishnadasan, A.; Gorwitz, R. J.; Fosheim, G. E.; McDougal, L. K.; Carey, R. B.; Talan, D. A. Methicillin-

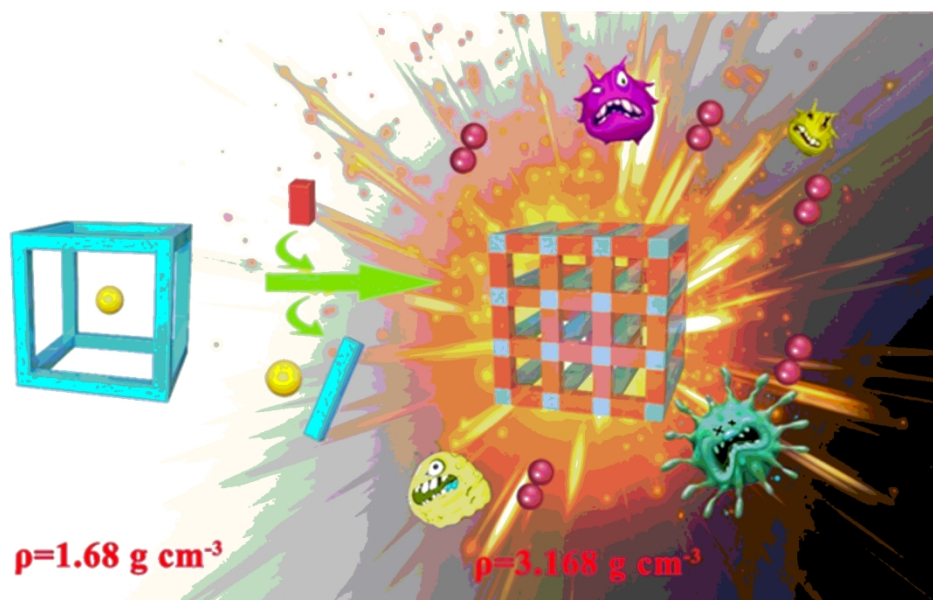
Resistant *S. Aureus* Infections Among Patients in the Emergency Department, *N. Engl. J. Med.*, **2006**, 355:666-674.

(48) Kaper, J. B.; Nataro, J. P.; Mobley, H. L. Pathogenic *Escherichia Coli*, *Nat. Rev. Microbiol.*, **2004**, 2, 123-140.

(49) Bodey, G. P.; Bolivar, R.; Fainstein, V.; Jadeja, L. Infections Caused by *Pseudomonas Aeruginosa*, *Rev. of infectious diseases*, **1983**, 5(2): 279-313.

TOC Graphic





150x90mm (300 x 300 DPI)